International Journal of Fatigue 119 (2019) 52–61

Contents lists available at ScienceDirect

International Journal of Fatigue

journal homepage: www.elsevier.com/locate/ijfatigue

Fatigue crack nucleation and small crack growth in an extruded 6061 aluminum alloy

R.R. McCullough[a], J.B. Jordon[a,*], P.G. Allison[a,b], T. Rushing[b], L. Garcia[b]

[a] Dept. of Mechanical Engineering, The University of Alabama, Tuscaloosa, AL 35487, USA
[b] US Army Engineer Research and Development Center, Geotechnical and Structures Laboratory, 3909 Halls Ferry Rd., Vicksburg, MS 39180, USA

ARTICLE INFO

Keywords:
Fatigue
Fatigue crack nucleation
Small crack growth
Micromechanical simulations
Modeling
Aluminum alloy

ABSTRACT

A combined synergistic experimental and computational approach has been employed to elucidate the underlying mechanisms for fatigue crack nucleation and microstructurally small crack growth in a 6061 aluminum alloy as a function of two heat treatments: a T6 treatment in its as-received state and a custom annealing condition. In this study, fully-reversed fatigue experiments of the 6061 aluminum alloy in two heat treatment conditions were performed in strain-control. Post-mortem analyses of the fracture surfaces were conducted to quantify sources of crack nucleation and microstructurally small crack growth. In particular, striation spacing in the small crack stage was measured up to the point of nucleation at cracked intermetallic particles and/or clusters of cracked particles. To capture the mechanics of fatigue crack nucleation, the local strain field at cracked intermetallic particles were estimated using micromechanics finite element simulations. Both the finite element approach and the experimental results were used in the implementation of a multi-stage fatigue model in order to correlate the microstructure-influenced mechanical response, including fatigue crack nucleation and small crack propagation contributions on fatigue behavior in 6061 aluminum alloy under two heat treatments.

1. Introduction

Solution hardenable aluminum alloys in the 6XXX series are widely implemented into a variety of service conditions due to their manufacturability and excellent manufacturing properties [1]. Of these alloys, heat treatable aluminum-magnesium-silicon alloys are widely used due to their versatile collection of properties that make them ideal structural materials [2,3]. These properties include intermediate mechanical strength, strong corrosion resistance, excellent strength-to-weight ratios and good formability, which can be attributed to the presence of multi-scale sized precipitants, containing primarily magnesium and silicon alloying elements [4].

Like many polycrystalline metallic materials, failure due to fatigue is an important aspect of material behavior requiring extensive testing and analysis. The fatigue performance of aluminum alloys is affected by both extrinsic factors, such as thermal environment [5–8] and loading history [6,9–11], along with intrinsic factors including grain size, crystallographic orientations, inclusion morphology, void morphology, and magnitude of damage accumulation [11–17]. The formation of fatigue cracks within these materials has been well established as the coordinated progression of four distinct stages, including fatigue crack incubation, microstructurally small crack growth, physically small crack growth, and long crack growth [18,19].

Of late, this paradigm has seen extensive use in the application of the multi-stage fatigue (MSF) model [20]. The microstructurally-sensitive MSF model was developed to capture the fatigue behavior of cast A356-T6 aluminum alloy based on the intrinsic structural properties of porosity, hard silicate precipitates, and spatial orientations of these features [21,22]. The MSF was later extended for other cast alloys including hexagonal close pack (HCP) AE44 and AM50 magnesium alloys [23,24]. Furthermore, the MSF model was expanded to incorporate non-porosity dominated metals, such as wrought Al-Zn-Mg aluminum alloys (AA7075) and AA6061-SiC metal matrix composites, where cracks nucleated from intermetallic and reinforcing particles that were homogenously distributed throughout the aluminum matrix [25–27]. In addition, the MSF model captured the performance of additive manufacturing steels, including Laser Engineered Net Shaping (LENS™)-processed 316L steel and FC-0205 steel, where large porosity created a limited, microstructurally small crack growth contribution to total fatigue life [28–30]. The MSF model was also shown to be effective in capturing the fatigue behavior of acrylonitrile butadiene styrene (ABS) copolymer and demonstrated that the multi-stage paradigm used for metallic alloys was also effective for polymers [31].

The focus of the present study is to capture the mechanisms of

* Corresponding author.
E-mail address: bjordon@eng.ua.edu (J.B. Jordon).

https://doi.org/10.1016/j.ijfatigue.2018.09.023
Received 25 September 2017; Received in revised form 21 September 2018; Accepted 23 September 2018
Available online 24 September 2018

observed multi-stage fatigue crack nucleation and growth in Al-Mg-Si alloy (AA6061). While just a few experimental studies on the low cycle fatigue performance of AA6061 exist [32,33], to the best of the author's knowledge, this is the first study to examine the fatigue crack nucleation and microstructurally small crack growth mechanisms of AA6061 through both experimental and numerical methods.

2. Materials and experimental procedures

2.1. Materials and specimens

The as-received material used in this study is a wrought Al-0.1%Mg-0.7%Si aluminum alloy (AA6061) produced by Taber Extrusion of Arkansas, USA, as extruded rail stock in T6 heat treatment condition. For fatigue testing, a modified ASTM E606-92 cylindrical fatigue specimen, aligned relative to extrusion direction, was used that incorporated a shorter gage section and increased cross-sectional area for the purpose of eliminating the potential of buckling of the specimen during high compressive strain amplitudes. The gage length and diameter of the dog-bone shaped specimens were 15 mm and 8 mm, respectively. All specimen gage sections were polished with 320 grit silicon carbide paper along the longitudinal axis to remove radial featured and machining defects.

Literature has established that aluminum alloys, specifically AA6061, when exposed to elevated thermal environments can exhibit a reduction in mechanical properties, including tensile strength and elastic modulus [34–36]. Therefore, to study the mechanical and microstructural influence of AA6061 in a thermally affected state, a custom designed heat treatment schedule was developed according to a military specific rapid rate boundary condition [34,37]. For this custom annealing process, a Carbolite ELF 11/23 box furnace was utilized to obtain a 316 °C ambient air, thermal environment. The temperature exposure of the AA6061 included ramp and hold times of approximately 960 ± 10 s and 440 ± 20 s, respectively. The interval between the heat treatment and placement on the cooling rack was approximately 1 min. The specimens were cooled at ambient room temperature (24.4 °C) for 20 min. An Extech SDL200 thermocouple meter calibrated to NIST standards was utilized to record ambient, local, and material reference temperatures during the annealing process. For discussion purposes in this paper, the modified annealing processed material is referred to as "annealed."

2.2. Mechanical testing

A MTS servo-hydraulic load frame was used to performed strain-controlled ambient temperature uniaxial monotonic experiments at a strain rate of 0.001/s until fracture. Additionally, a MTS servo-hydraulic load frame was used to conduct strain-controlled fatigue experiments under fully reversed (R = −1) conditions at room temperature and relative humidity (T = 24.4 °C and H = 42%). The fatigue tests were conducted at a frequency of 5 Hz using a fatigue-rated MTS extensometer with a 10-mm gauge length. Final failure of the specimen was defined as a 50% drop in peak load during the test. The fatigue experiments were performed in triplicate for strain amplitudes between 0.1% and 1%. However, due to a limited number of specimens available, only a single test was performed for strain amplitudes between 1.25% and 2.5% for both T6 and annealed conditions.

2.3. Microstructure characterization

Optical and electron microscopy techniques characterized the AA6061 microstructure in both the T6 and annealed condition. Microstructure characterization of the specimens were prepared by cutting along the longitudinal (L) and long transverse (LT) planes in order to expose the microstructure aligned with the extrusion direction. Specimens were then mounted using a cold mount resin and polished using a diamond suspension down to 0.5 μm, with final polishing consisting of 50 nm colloidal silica. The samples were ultrasonically cleaned in ethanol to remove any clinging polishing particulates between polishing steps. An etching technique after polishing [38] was used to produce highly contrasted grain boundaries and precipitate sites. The first step was composed of pre-etching for 30 s in a solution of 1 g NaCl in 50 mL of H3PO4. The second step then included etching for 6 s with Weck's reagent (1 g NaOH and 4 g KMnO4 in 100 mL of H2O). The entire etching process was conducted at room temperature, and the specimens were regularly cleaned with critical detergent to remove excess solution from the etched surface. For optical imaging, a Keyence VHX-2000 Digital microscope with a VH-Z100 lens was employed. While for high magnification electron imaging, a JEOL 7000 series field emission scanning electron microscope equipped with an Oxford X-Max Silicon Drift Energy Dispersive X-ray (EDX) Detector was employed for investigating the initial microstructure and fracture surface morphology.

3. Experimental results and discussion

3.1. Microstructure

Chemically etched optical micrographs of the AA6061 in the as-received T6 and annealed states are shown in Fig. 1. The etching assisted in the definition of the intermetallic particles suspended within the matrix. The elongated nature of the extrusion texture can be clearly seen in the microstructure in both states. Small, elongated grains were observed throughout the T6 state, with some larger particles located near the edges of the material, which is consistent with extruded Al-Mg-Si alloys [39]. Slightly larger grains were noted in geometrically equivalent zones within the annealed condition. Particle stringers were observed in the AA6061 in the direction of extrusion in both conditions.

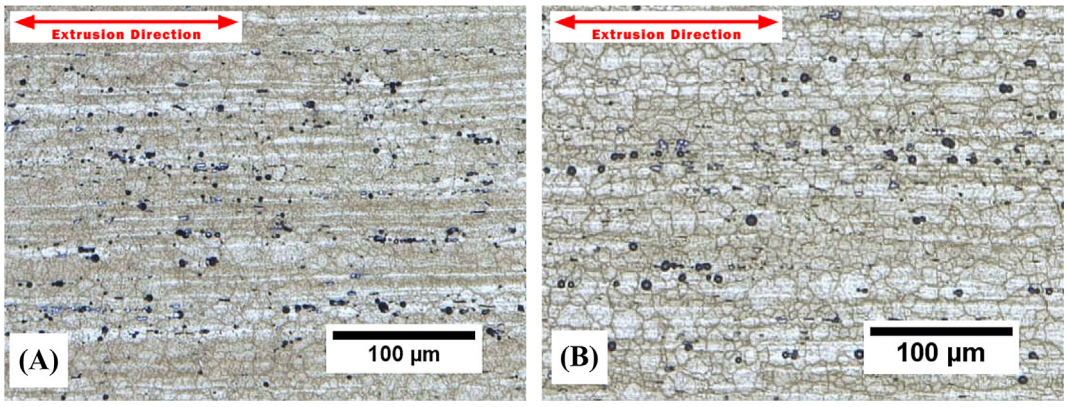

Fig. 1. Optical images of etched (A) as-received (T6) and (B) annealed AA6061.